Research Article | Vol. 29, No. 19 / 13 Sep 2021 / Optics Express 30579
Optics EXPRESS

Linear-polarization metasurface converter with an arbitrary polarization rotating angle

XIAOYI WANG[1] AND GUO-MIN YANG[2,*]

[1] Poly-grames Research Center, Polytechnique Montréal, Montréal, H3T 1J4, Canada
[2] Key Laboratory for Information Science of Electromagnetic Waves, School of Information Science and Technology, Fudan University, Shanghai, 200433, China
[*] guominyang@fudan.edu.cn

Abstract: This paper presents a new design of linear-polarization metasurface converter with arbitrary polarization rotating angle. The linear-polarization conversion is achieved by first separating the linearly polarized incident wave into two orthogonal circularly polarized waves, then adding an additional phase to one of the circularly polarized waves, and finally recombining these two circularly polarized waves into a linearly polarized wave and reflecting it towards free space. A practical unit cell operating at 10 GHz with sandwich structure is applied to realize the linear-polarization metasurface converter, which consists of a top-layer square patch, a middle-layer ground plane, a bottom-layer 90° quadrature hybrid coupler, and two vias connecting the top layer and bottom layer. The proposed linear-polarization metasurface converter is analyzed theoretically and demonstrated by both simulating and experimental results.

1. Introduction

Metasurfaces, the two-dimensional equivalent of bulky three-dimensional metamaterials, have been becoming a revolutionary technology in electromagnetic wave manipulation, due to their natural benefits of low-profile, low-cost, easy-fabrication and the flexible capability of electromagnetic wave transformation [1]. A variety of metasurface based applications have been reported, such as electromagnetic wavefront shaping [2–9], energy absorption [10–12], holography [13,14], analog mathematical computing [15], cloaking [16–18], camouflaging [19,20], nonreciprocity [21,22], frequency conversion [23,24], and simplified wireless communication and radar systems [25–29].

Manipulating the polarization of electromagnetic waves is crucial in many practical scenarios, such as radar cross-section (RCS) reduction [30,31], wireless communication [32–34], high-resolution imaging [35], and liquid crystal display (LCD) [36]. Conventionally, the polarization of an electromagnetic wave is controlled through the devices such as dichroic glasses, birefringent wave plates, and liquid crystals, which are generally bulky and have limited operating bandwidth [37–39], thus limiting their capability of integration within practical applications. Thanks to the attractive features of metasurfaces, a diversity of polarization converters have been studied using metasurface technology [37–48]. Nevertheless, most of the polarization converting metasurfaces are implemented by achieving desired resonating states for specified polarized incident waves, resulting in certain amplitude and phase responses and then further converting their scattering polarization, which usually have fixed functions with less flexibility.

In this paper, we propose a new design of metasurface based linear polarization (LP) converter. Different from conventional metasurface based polarization converters, the realization of proposed LP rotation may be divided into three steps: First, separating the LP incident wave into two waves with different circular polarization (CP), namely, left-hand circular polarization (LHCP) and right-hand circular polarization (RHCP). Second, introducing an additional phase to one of the CP waves, and finally recombining the two CP waves and radiating back to free space. During this procedure, the polarization rotating angle is fully determined by the additional phase

#436322 https://doi.org/10.1364/OE.436322
Journal © 2021 Received 7 Jul 2021; revised 29 Aug 2021; accepted 30 Aug 2021; published 7 Sep 2021

Optics EXPRESS

introduced in the second step, and the rotating direction is controlled by adding the additional phase to the selected CP component. Those features make the proposed LP metasurface converter easy to achieve arbitrary angle rotation and arbitrary rotating direction by simply changing the value of added phase and switching the CP component to add the additional phase. What's more, the proposed LP metasurface converter is insensitive to incident LP direction.

The rest of this paper is organized as follows. Section 2 establishes the general principle of the proposed LP metasurface converter. Then, section 3 presents a practical metasurface realization using a square patch and a quadrature hybrid coupler [49]. Next, section 4 provides the full-wave simulation results of the designed metasurface, and section 5 fabricates the designed metasurface and demonstrates the proposed design by experiment. Finally, section 7 concludes this paper.

2. Principle

Figure 1 provides the conceptual illustration of a reflective LP metasurface converter. A linearly polarized incident wave at frequency ω_0, $\psi_i(t, \omega_0)$, whose electric field is $\boldsymbol{E}_i(t)$, impinges on the metasurface based polarization converter. The linearly polarized wave interacts with the metasurface and is reflected back to the free space. The LP of the scattered wave $\psi_r(t, \omega_0)$ is rotated by an angle of θ, with the electric field $\boldsymbol{E}_r(t)$.

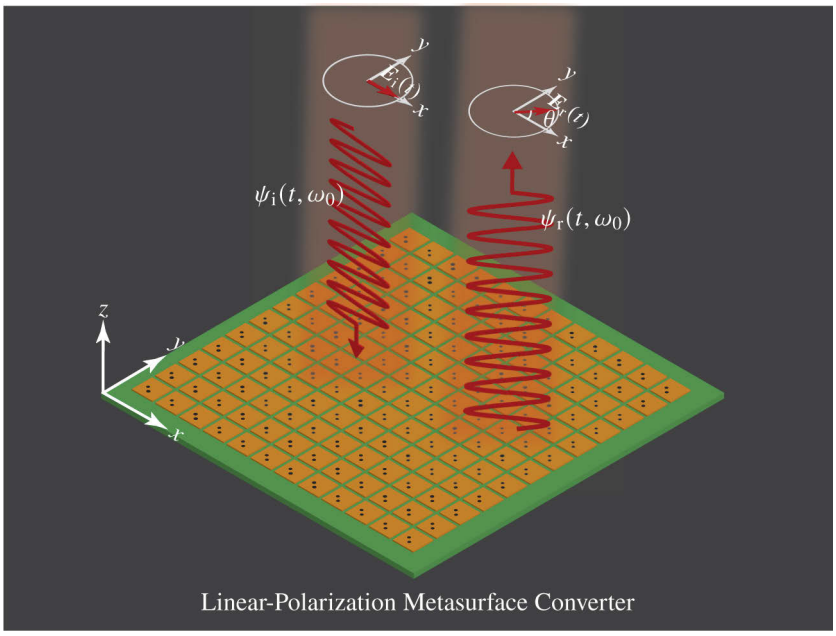

Fig. 1. The conceptual illustration of proposed reflective linear polarization (LP) metasurface converter with a reflecting rotating angle θ.

Figure 2 explains the general operating principle of the LP metasurface converter. An incident linearly polarized harmonic wave $\boldsymbol{\psi}_i(t)$ whose LP is in the $\boldsymbol{x}$ direction, namely,

$$\boldsymbol{\psi}_i(t) = \sin(\omega_0 t)\boldsymbol{x}, \tag{1}$$

impinges on the LP metasurface converter. The linearly polarized incident wave $\boldsymbol{\psi}_i(t)$ may be divided into two orthogonal circularly polarized waves, LHCP and RHCP, respectively,

$$\boldsymbol{\psi}_i(t) = \left[\frac{1}{2}\sin(\omega_0 t)\boldsymbol{x} + \frac{1}{2}\cos(\omega_0 t)\boldsymbol{y}\right] + \left[\frac{1}{2}\sin(\omega_0 t)\boldsymbol{x} - \frac{1}{2}\cos(\omega_0 t)\boldsymbol{y}\right], \tag{2}$$

Optics EXPRESS

where the terms in the first pair of square brackets represent the RHCP wave and the terms in the second pair of square brackets represent the LHCP wave.

The metasurface interacts with the incident wave and adding an additional phase ϕ to one of the CP waves. If the additional phase ϕ is added to the RHCP wave, the reflected wave may be expressed as

$$\begin{aligned}\boldsymbol{\psi}_{\mathrm{r}}(t) &= \left[\frac{1}{2}\sin(\omega_0 t-\phi)\boldsymbol{x}+\frac{1}{2}\cos(\omega_0 t-\phi)\boldsymbol{y}\right]+\left[\frac{1}{2}\sin(\omega_0 t)\boldsymbol{x}-\frac{1}{2}\cos(\omega_0 t)\boldsymbol{y}\right]\\ &=\left[\frac{1}{2}\sin(\omega_0 t-\phi)+\frac{1}{2}\sin(\omega_0 t)\right]\boldsymbol{x}+\left[\frac{1}{2}\cos(\omega_0 t-\phi)-\frac{1}{2}\cos(\omega_0 t)\right]\boldsymbol{y}\\ &=\sin(\omega_0 t-\frac{\phi}{2})\cos(\frac{\phi}{2})\boldsymbol{x}+\sin(\omega_0 t-\frac{\phi}{2})\sin(\frac{\phi}{2})\boldsymbol{y}\\ &=\sin(\omega_0 t-\frac{\phi}{2})\left[\cos(\frac{\phi}{2})\boldsymbol{x}+\sin(\frac{\phi}{2})\boldsymbol{y}\right].\end{aligned} \tag{3}$$

The expression in the last equality of (3) shows that the reflected wave contains not only the $\boldsymbol{x}$ component but also $\boldsymbol{y}$ component. These two components are in phase but have different amplitudes, which demonstrates that the reflected wave is still linearly polarized but with a rotated angle. The polarization rotating angle θ may be simply derived by comparing the values of components in $\boldsymbol{x}$ and $\boldsymbol{y}$ directions,

$$\theta=\tan^{-1}\left(\frac{\sin\frac{\phi}{2}}{\cos\frac{\phi}{2}}\right)=\frac{\phi}{2}. \tag{4}$$

Similarly, If the additional phase ϕ is added to LHCP, the reflected wave is expressed as

$$\begin{aligned}\boldsymbol{\psi}_{\mathrm{r}}(t) &= \left[\frac{1}{2}\sin(\omega_0 t)\boldsymbol{x}+\frac{1}{2}\cos(\omega_0 t)\boldsymbol{y}\right]+\left[\frac{1}{2}\sin(\omega_0 t-\phi)\boldsymbol{x}-\frac{1}{2}\cos(\omega_0 t-\phi)\boldsymbol{y}\right]\\ &=\left[\frac{1}{2}\sin(\omega_0 t)+\frac{1}{2}\sin(\omega_0 t-\phi)\right]\boldsymbol{x}+\left[\frac{1}{2}\cos(\omega_0 t)-\frac{1}{2}\cos(\omega_0 t-\phi)\right]\boldsymbol{y}\\ &=\sin(\omega_0 t-\frac{\phi}{2})\cos(\frac{\phi}{2})\boldsymbol{x}-\sin(\omega_0 t-\frac{\phi}{2})\sin(\frac{\phi}{2})\boldsymbol{y}\\ &=\sin(\omega_0 t-\frac{\phi}{2})\left[\cos(\frac{\phi}{2})\boldsymbol{x}-\sin(\frac{\phi}{2})\boldsymbol{y}\right].\end{aligned} \tag{5}$$

Then, the polarization rotating angle θ is obtained as

$$\theta=\tan^{-1}\left(\frac{-\sin\frac{\phi}{2}}{\cos\frac{\phi}{2}}\right)=-\frac{\phi}{2}. \tag{6}$$

Equation (4) and (6) show that the LP rotating angle θ is half of the added additional phase ϕ, and the rotating direction depends on which CP component ϕ is added. Since any linearly polarized wave can be naturally divided into two orthogonal circularly polarized wave as seen in (2), the theory here is perfectly valid for any linearly polarized incident wave with arbitrary polarization angle.

Optics EXPRESS

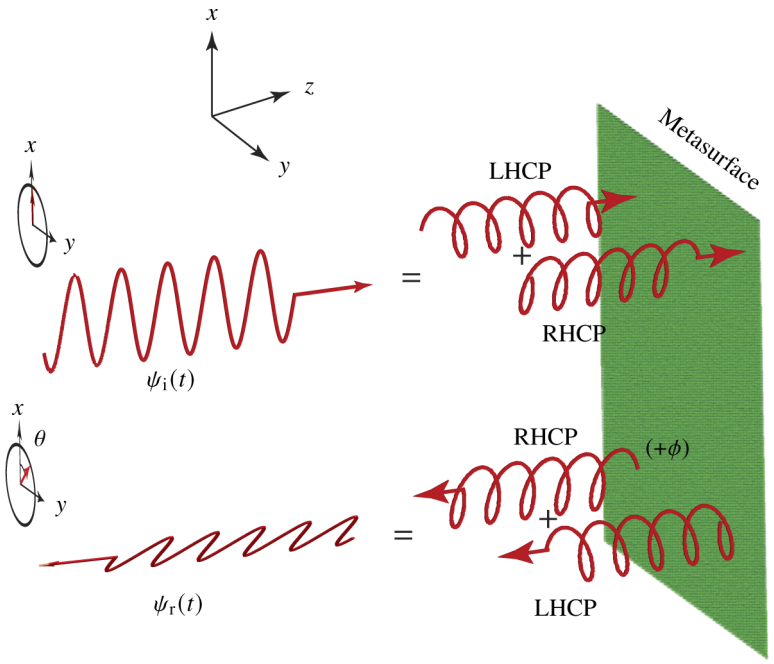

Fig. 2. Principle of proposed arbitrary linear-polarization metasurface converter, where an incident linearly polarized wave $\psi_i(t)$ with $\boldsymbol{x}$ polarization is divided into two circularly polarized waves, the two waves experience different reflective phases (RHCP experiences ϕ more phase shift than LHCP in this figure) and are recombined into a linearly polarized wave $\psi_r(t)$ with a rotated polarization angle θ.

3. Metasurface unit cell design

A practical metasurface structure is designed to realize the proposed LP metasurface converter. Figure 3 depicts the layout of the metasurface unit cell with designing parameters. Figure 3(a) shows the side view of the unit cell, which is a sandwich structure formed by two Rogers 6002 substrates, whose dielectric constant is 2.94 and dissipation factor is 0.0012. It consists of a top layer metallic patch, a middle layer ground plane, a bottom layer circuit, and two metalized vias connecting the top and bottom layers. Figure 3(b) shows the top layer structure. It is a square patch with two feeding points, corresponding to the two orthogonal LP feeding positions, which are connected to the bottom layer through the two vias. The square patch is designed to be resonant at 10 GHz, so it can perfectly pick up the two orthogonal LP incident waves with $\boldsymbol{x}$ and $\boldsymbol{y}$ polarization at the two feeding points, respectively. Figure 3(c) shows the middle ground layer. It contains two circular slots on the ground to avoid shorting the two vias, which are connecting the top and bottom layers, to the ground. Figure 3(d) shows the bottom circuit layer. Its main part is a typical 4-port 90° quadrature hybrid coupler with the following form scattering parameter matrix $[S_c]$ [49]:

$$[S_c] = -\frac{1}{\sqrt{2}}\begin{bmatrix} 0 & j & 1 & 0 \\ j & 0 & 0 & 1 \\ 1 & 0 & 0 & j \\ 0 & 1 & j & 0 \end{bmatrix}. \tag{7}$$

Optics EXPRESS

Ports 2 and 3 of the coupler are connected to the two feeding points on the top patch layer through the vias, respectively. As a result, port 1 of the coupler receives the RHCP component of the LP incident wave, as $S_{12} = -j\frac{1}{\sqrt{2}}$, $S_{13} = -\frac{1}{\sqrt{2}}$, and port 4 of the coupler receives the LHCP component of the LP incident wave, as $S_{42} = -\frac{1}{\sqrt{2}}$, $S_{43} = -j\frac{1}{\sqrt{2}}$, hence, the two CP components in the incident wave are separated in ports 1 and 4 of the coupler. The additional phase ϕ added in one of the CP components for polarization rotation may be simply realized by adding an open-end microstrip line with the length,

$$\Delta L = \frac{\phi}{2k_0}, \tag{8}$$

in corresponding CP ports, where k_0 is the wave number of the guided wave in the microstrip line. Namely, $L_1 = \Delta L, L_2 = 0$ are chosen for clockwise polarization rotation and $L_2 = \Delta L, L_1 = 0$ are chosen for anticlockwise rotation. The factor of $\frac{1}{2}$ in ΔL is due to the fact that the open-end microstrip line works as a reflective phase shifter and therefore exhibits a double phase of $k_0\Delta L$. The waves reflected by the open-end microstip line and coupler are recombined on the top patch layer and reradiated to free space with a rotated polarization angle.

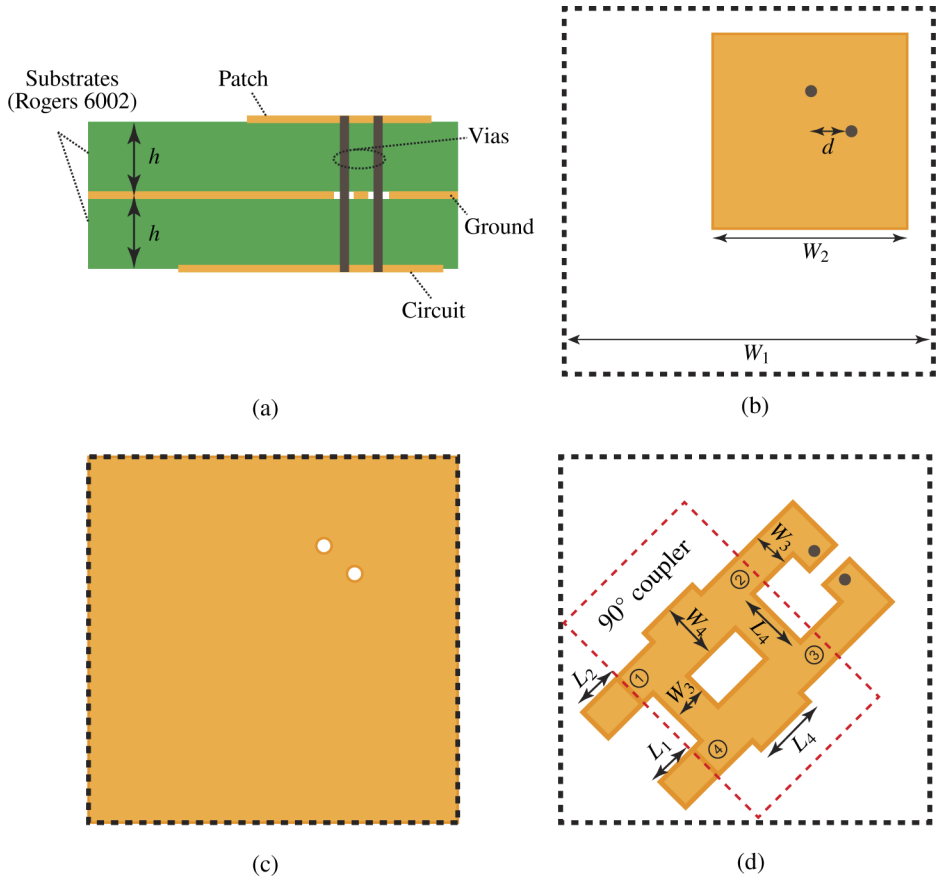

Fig. 3. Metasurface unit cell realization with design parameters ($h = 0.76$ mm, $W_1 = 15.0$ mm, $W_2 = 8.2$ mm, $W_3 = 1.93$ mm, $d = 1.78$ mm, $L_4 = 3.63$ mm, $W_4 = 3.25$ mm). (a) Side view. (b) Top layer. (c) Middle layer. (d) Bottom layer.

Optics EXPRESS

4. Full-wave simulation results

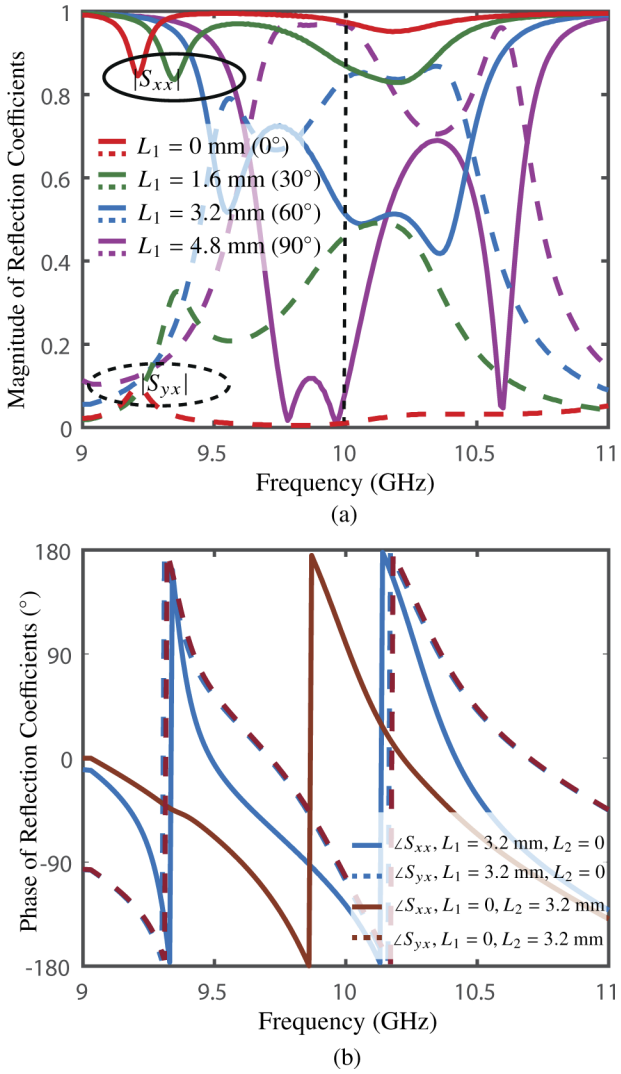

Fig. 4. Scattering parameters from full-wave simulation. (a) Magnitudes of reflection coefficients for different L_1, when $L_2 = 0$. (b) Phases of reflection coefficients for the cases $L_1 = 0$ and $L_2 = 0$.

Figure 4 plots the full-wave simulation results of the proposed LP metasurface converter design with the help of Ansys Electronics. Figure 4(a) plots the magnitudes of the co-polarized and cross-polarized reflection coefficients, $|S_{xx}|$ and $|S_{yx}|$, for different L_1 when L_2 is fixed to 0, where different L_1 is corresponding to different phase shift θ added to the RHCP component, as shown in Fig. 2. It shows that when L_1 increases from 0, corresponding to 0°, to 4.8 mm, corresponding to 90°, $|S_{xx}|$ reduces from 1 to 0, while $|S_{yx}|$ increases from 0 to 1, approximately, which demonstrates that the amount of ***y***-polarized scattered wave converted from incident ***x***-polarized wave by the LP metasurface converter increases as L_1 increases, and hence the reflected linealy polarized wave rotating angle θ increases. Similarly, if L_1 is fixed to 0, different L_2 is corresponding to different phase shift θ added to the LHCP component, as shown in Fig. 2.

Optics EXPRESS

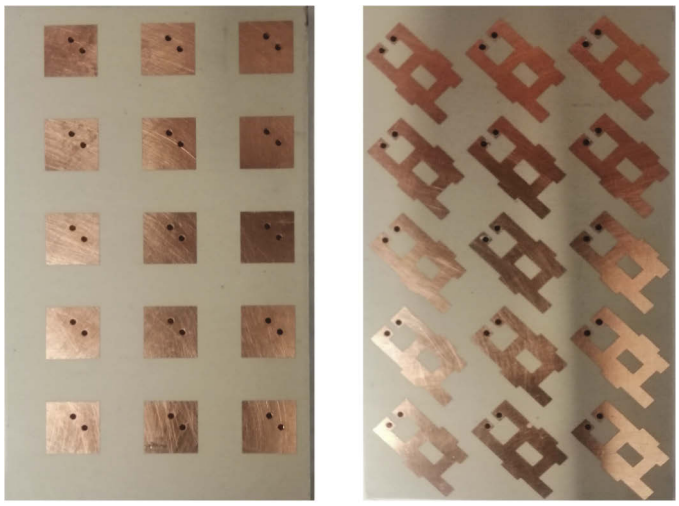

(a) (b)

Fig. 5. Fabricated prototype of the proposed LP metasurface converter. (a) Top view. (b) Bottom view.

Figure 4(b) plots the phases of co-polarized and cross-polarized reflection coefficients, $\angle S_{xx}$ and $\angle S_{yx}$, for the two cases $L_1 = 3.2$ mm, $L_2 = 0$ and $L_1 = 0, L_2 = 3.2$ mm. It shows that the co-polarized and cross-polarized reflected waves are approximately in phase when $L_2 = 0$ mm, and out of phase when $L_1 = 0$ mm, which demonstrates that in both cases the polarization of reflected waves are linear. However, when $L_1 = 2.4$ mm, the reflected LP rotates clockwise, while when $L_2 = 0$ mm, the reflected LP rotates anticlockwise.

5. Experimental demonstration

A LP metasurface converter with 3×5 elements and reflected polarization rotating phase $\theta = 45°$ is designed and fabricated based on the proposed concept. In order to achieve the designed rotating angle θ, $L_1 = 2.4$ mm and $L_2 = 0$ mm in Fig. 3 are chosen to design the LP metasurface converter. Figure 5 presents the fabrication prototype of the LP metasurface converter, where Fig. 5(a) shows the top view and Fig. 5(b) shows the bottom view of the LP metasurface converter prototype.

Fig. 6 provides the experimental demonstration of the fabricated LP metasurface converter. Figure 6(a) shows the experimental setup. The testing LP metasurface converter is placed in front of a piece of absorbing material. A pair of linearly polarized antennas are chosen as the transmitting and receiving antennas, respectively. The distance between the antennas and the metasurfce converter is around 80 cm. The two excitation ports of the two antennas are connected to a vector network analyzer (VNA) to measure the scattering parameters. During the measurement, the transmitting antenna is fixed, while the receiving antenna is set to have the same polarization direction as the transmitting antenna in the initial stage and then the receiving antenna is rotated manually with the rotating angle α to measure the scattered wave. Figure 6(b) plots the measured normalized $|S_{21}|$ against different rotating angles α of the receiving antenna and its comparison with ideal and full-wave simulated results. The measured results is plotted with interpolation using least square method. It shows that the measured result agrees with the ideal and simulated results. When $\alpha = 42.2°$, the measured $|S_{21}|$ arrives the maximum, which is very closed to the designed value 45° and demonstrates the proposed concept and design. The small deviation of LP rotating angle may be introduced by the fabrication resolution, the

Optics EXPRESS

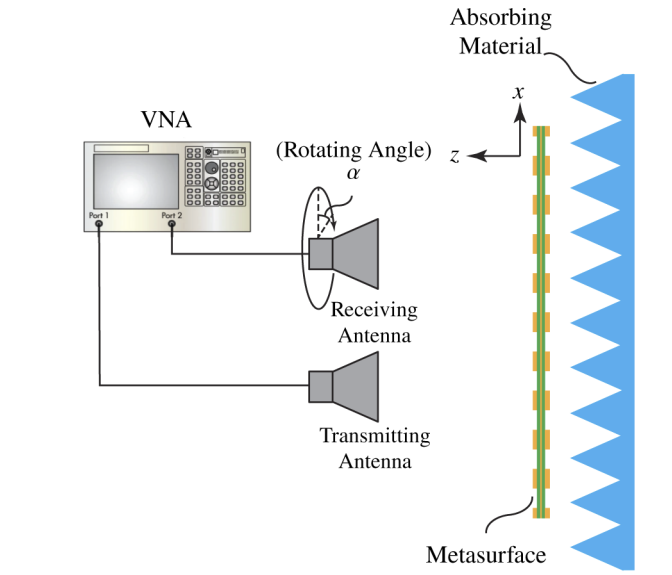

(a)

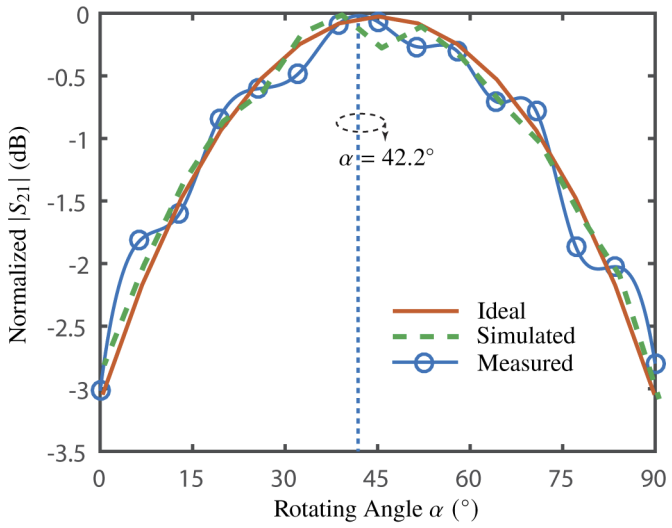

(b)

Fig. 6. Experimental demonstration of proposed LP metasurface converter. (a) Experimental setup. (b) Comparison between ideal, simulated and measured normalized $|S_{21}|$ for different receiving antenna rotating angles α.

Optics EXPRESS

undesired scattering from the surrounding environment, and the edge effect of the metasurface with a finite size.

6. Comparison and discussion

Finally, the comparison between this work and other reported works is provided in Table 1. It is clearly observed that different from other works that are based on the different resonating states for different incident components, the proposed LP metasurface converter is realized with the antenna-circuit-antenna design, which separates the process of incidence picking up and wave processing, leading to flexible LP rotating angle.

Table 1. Comparison between reported work and this work.

Work	Method	LP Rotating angle
Ref. [39]	Resonating Structure	90°
Ref. [42]	Resonating Structure	90°
Ref. [42]	Resonating Structure	90°
Ref. [46]	Resonating Structure	90°
This work	Antenna-Circuit-Antenna	Arbitary

In addition, it is worth mentioning that the operating band and bandwidth of the proposed LP metasurface converter are fully determined by the operating bands and bandwidth of the microstrip antenna and the 90° hybrid coupler. By designing wideband or multiple band picking-up antenna and coupler components using various modern technologies [49,50], the operating band and bandwidth may be further improved.

7. Conclusion

We have presented a new design of LP metasurface converter. This LP metasurface converter is insensitive to incident wave polarization direction and may be easily implemented to achieve arbitrary polarization rotating angle by adjusting the additional microstrip line length connecting to the coupler ports. The proposed LP metasurface converter is analyzed theoretically and demonstrated by both full-wave simulation and experimental verification. This LP metasurface converter may find wide potential applications in RCS reduction, wireless communication, and imaging systems.

Funding. National Key Research and Development Program of China (2017YFA0100203).

Disclosures. The authors declare no conflicts of interest.

Data availability. Data underlying the results presented in this paper are not publicly available at this time but may be obtained from the authors upon reasonable request

References

1. K. Achouri and C. Caloz, *Electromagnetic Metasurfaces: Theory and Applications* (Wiley-IEEE, 2021).
2. B. Han, S. Li, Z. Li, G. Huang, J. Tian, and X. Cao, "Asymmetric transmission for dual-circularly and linearly polarized waves based on a chiral metasurface," Opt. Express **29**(13), 19643–19654 (2021).
3. S. J. Li, Y. B. Li, L. Zhang, Z. J. Luo, B. W. Han, R. Q. Li, X. Y. Cao, Q. Cheng, and T. J. Cui, "Programmable controls to scattering properties of a radiation array," Laser Photonics Rev. **15**(2), 2000449 (2021).
4. S. J. Li, Y. B. Li, H. Li, Z. X. Wang, C. Zhang, Z. X. Guo, R. Q. Li, X. Y. Cao, Q. Cheng, and T. J. Cui, "A thin self-feeding janus metasurface for manipulating incident waves and emitting radiation waves simultaneously," Ann. Phys. (Berl.) **532**(5), 2000020 (2020).
5. K. Chen, Y. Feng, Z. Yang, L. Cui, J. Zhao, B. Zhu, and T. Jiang, "Geometric phase coded metasurface: from polarization dependent directive electromagnetic wave scattering to diffusion-like scattering," Sci. Rep. **6**(1), 35968 (2016).

Optics EXPRESS

6. C. Pfeiffer and A. Grbic, "Controlling vector bessel beams with metasurfaces," Phys. Rev. Appl. **2**(4), 044012 (2014).
7. M. Liu, D. A. Powell, Y. Zarate, and I. V. Shadrivov, "Huygens' metadevices for parametric waves," Phys. Rev. X **8**, 031077 (2018).
8. F. Zhang, Q. Song, G.-M. Yang, and Y.-Q. Jin, "Generation of wideband vortex beam with different oam modes using third-order meta-frequency selective surface," Opt. express **27**(24), 34864–34875 (2019).
9. K. Zhang, Y. Wang, S. N. Burokur, and Q. Wu, "Generating dual-polarized vortex beam by detour phase: From phase gradient metasurfaces to metagratings," *IEEE Trans. Microw. Theory Techn.* pp. 1–10 (2021).
10. M. Li, L. Guo, J. Dong, and H. Yang, "An ultra-thin chiral metamaterial absorber with high selectivity for LCP and RCP waves," J. Phys. D **47**(18), 185102 (2014).
11. Y. Wen, W. Ma, J. Bailey, G. Matmon, X. Yu, and G. Aeppli, "Planar broadband and high absorption metamaterial using single nested resonator at terahertz frequencies," Opt. Lett. **39**(6), 1589–1592 (2014).
12. T. Deng, J. Liang, T. Cai, C. Wang, X. Wang, J. Lou, Z. Du, and D. Wang, "Ultra-thin and broadband surface wave meta-absorber," Opt. Express **29**(12), 19193–19201 (2021).
13. G. Zheng, H. Mühlenbernd, M. Kenney, G. Li, T. Zentgraf, and S. Zhang, "Metasurface holograms reaching 80% efficiency," Nat. Nanotechnol. **10**(4), 308–312 (2015).
14. W. Ye, F. Zeuner, X. Li, B. Reineke, S. He, C.-W. Qiu, J. Liu, Y. Wang, S. Zhang, and T. Zentgraf, "Spin and wavelength multiplexed nonlinear metasurface holography," Nat. Commun. **7**(1), 11930 (2016).
15. A. Silva, F. Monticone, G. Castaldi, V. Galdi, A. Alù, and N. Engheta, "Performing mathematical operations with metamaterials," Science **343**(6167), 160–163 (2014).
16. A. Alù, "Mantle cloak: Invisibility induced by a surface," Phys. Rev. B **80**(24), 245115 (2009).
17. N. M. Estakhri and A. Alù, "Ultra-thin unidirectional carpet cloak and wavefront reconstruction with graded metasurfaces," IEEE Antennas Wirel. Propag. Lett **13**, 1775–1778 (2014).
18. D. Ramaccia, D. L. Sounas, A. Alù, A. Toscano, and F. Bilotti, "Doppler cloak restores invisibility to objects in relativistic motion," Phys. Rev. B **95**(7), 075113 (2017).
19. X. Wang and C. Caloz, "Spread-spectrum selective camouflaging based on time-modulated metasurface," IEEE Trans. Antennas Propag. **69**(1), 286–295 (2021).
20. X. Wang and C. Caloz, "Spacetime-modulated metasurface camouflaging," in *Proceedings of IEEE AP-S Int. Antennas Propag. (APS)*, (IEEE, 2020), pp. 963–964.
21. C. Caloz, A. Alù, S. Tretyakov, D. Sounas, K. Achouri, and Z.-L. Deck-Léger, "Electromagnetic nonreciprocity," Phys. Rev. Applied **10**(4), 047001 (2018).
22. L. Zhang, X. Q. Chen, R. W. Shao, J. Y. Dai, Q. Cheng, G. Castaldi, V. Galdi, and T. J. Cui, "Breaking reciprocity with space-time-coding digital metasurfaces," Adv. Mater. **31**(41), 1904069 (2019).
23. D. Ramaccia, D. L. Sounas, A. Alù, A. Toscano, and F. Bilotti, "Phase-induced frequency conversion and doppler effect with time-modulated metasurfaces," IEEE Trans. Antennas Propag. **68**(3), 1607–1617 (2020).
24. Z. Wu and A. Grbic, "Serrodyne frequency translation using time-modulated metasurfaces," IEEE Trans. Antennas Propag. **68**(3), 1599–1606 (2020).
25. J. Y. Dai, W. K. Tang, J. Zhao, X. Li, Q. Cheng, J. C. Ke, M. Z. Chen, S. Jin, and T. J. Cui, "Metasurfaces: Wireless communications through a simplified architecture based on time-domain digital coding metasurface," Adv. Mater. Technol. **4**(7), 1970037 (2019).
26. W. Tang, X. Li, J. Y. Dai, S. Jin, Y. Zeng, Q. Cheng, and T. J. Cui, "Wireless communications with programmable metasurface: Transceiver design and experimental results," China Commun. **16**(5), 46–61 (2019).
27. X. Wang and C. Caloz, "Direction-of-arrival (DoA) estimation based on spacetime-modulated metasurface," in *Proceedings of IEEE AP-S Int. Antennas Propag. (APS)*, (IEEE, 2019), pp. 1613–1614.
28. X. Wang and C. Caloz, "Spacetime-modulated metasurface for spatial multiplexing communication," in *Proceedings of 13th International Congress on Artificial Materials for Novel Wave Phenomena (Metamaterials)*, (IEEE, 2019), pp. 465–467.
29. X. Wang and C. Caloz, "Pseudo-random sequence (PRS) (space)time-modulated metasurfaces," engXiv. pp. 1–13 (2021).
30. Y. Zhao, X. Cao, J. Gao, X. Yao, T. Liu, W. Li, and S. Li, "Broadband low-RCS metasurface and its application on antenna," IEEE Trans. on Antennas Propag. **64**(7), 2954–2962 (2016).
31. Y. Jia, Y. Liu, Y. J. Guo, K. Li, and S. Gong, "A dual-patch polarization rotation reflective surface and its application to ultra-wideband rcs reduction," IEEE Trans. Antennas Propag. **65**(6), 3291–3295 (2017).
32. Y. Han and G. Li, "Coherent optical communication using polarization multiple-input-multiple-output," Opt. Express **13**(19), 7527–7534 (2005).
33. J. B. Mueller, N. A. Rubin, R. C. Devlin, B. Groever, and F. Capasso, "Metasurface polarization optics: independent phase control of arbitrary orthogonal states of polarization," Phys. Rev. Lett. **118**(11), 113901 (2017).
34. X. Wang and C. Caloz, "Phaser-based polarization-dispersive antenna and application to encrypted communication," in *Proceeding of IEEE AP-S Int. Antennas Propag. (APS)*, (IEEE, 2017), pp. 2187–2188.
35. A. Arbabi, Y. Horie, M. Bagheri, and A. Faraon, "Dielectric metasurfaces for complete control of phase and polarization with subwavelength spatial resolution and high transmission," Nat. Nanotechnol. **10**(11), 937–943 (2015).
36. R. H. Chen, *Liquid Crystal Displays: Fundamental Physics and Technology* (John Wiley & Sons, 2011).

Optics EXPRESS

37. S.-C. Jiang, X. Xiong, Y.-S. Hu, Y.-H. Hu, G.-B. Ma, R.-W. Peng, C. Sun, and M. Wang, "Controlling the polarization state of light with a dispersion-free metastructure," Phys. Rev. X **4**, 021026 (2014).
38. X. Xiong, S.-C. Jiang, Y.-S. Hu, Y.-H. Hu, Z.-H. Wang, R.-W. Peng, and M. Wang, "Control the polarization state of light with symmetry-broken metallic metastructures," Ann. Phys **358**, 129–158 (2015).
39. X. Huang, H. Yang, D. Zhang, and Y. Luo, "Ultrathin dual-band metasurface polarization converter," IEEE Trans. Antennas and Propag. **67**(7), 4636–4641 (2019).
40. L. Wu, Z. Yang, Y. Cheng, R. Gong, M. Zhao, Y. Zheng, J. Duan, and X. Yuan, "Circular polarization converters based on bi-layered asymmetrical split ring metamaterials," Appl. Phys. A **116**(2), 643–648 (2014).
41. B. Ren, Y. Feng, S. Tang, L. Wang, H. Jiang, and Y. Jiang, "Dynamic control of thz polarization modulation and multi-channel beam generation using a programmable metasurface," Opt. Express **29**(11), 17258–17268 (2021).
42. Z. Sun, B. Sima, J. Zhao, and Y. Feng, "Electromagnetic polarization conversion based on huygens' metasurfaces with coupled electric and magnetic resonances," Opt. Express **27**(8), 11006–11017 (2019).
43. N. A. Rubin, A. Zaidi, M. Juhl, R. P. Li, J. B. Mueller, R. C. Devlin, K. Leósson, and F. Capasso, "Polarization state generation and measurement with a single metasurface," Opt. Express **26**(17), 21455–21478 (2018).
44. F. Zhang, G.-M. Yang, and Y.-Q. Jin, "Design and analysis of linear to circular polarization converter with third-order meta-frequency selective surfaces," IEEE Trans. Antennas Propag. **68**(9), 6646–6655 (2020).
45. Y. Shi, H. X. Meng, and H. J. Wang, "Polarization conversion metasurface design based on characteristic mode rotation and its application into wideband and miniature antennas with a low radar cross section," Opt. Express **29**(5), 6794–6809 (2021).
46. H. Sun, C. Gu, X. Chen, Z. Li, L. Liu, and F. Martín, "Ultra-wideband and broad-angle linear polarization conversion metasurface," J. Appl. Phys. **121**(17), 174902 (2017).
47. Y. Yuan, S. Sun, Y. Chen, K. Zhang, X. Ding, B. Ratni, Q. Wu, S. N. Burokur, and C.-W. Qiu, "A fully phase-modulated metasurface as an energy-controllable circular polarization router," Adv. Sci. **7**(18), 2001437 (2020).
48. Z. Y. Li, S. J. Li, B. W. Han, G. S. Huang, Z. X. Guo, and X. Y. Cao, "Quad-band transmissive metasurface with linear to dual-circular polarization conversion simultaneously," Adv. Theory Simul. **4**(8), 2100117 (2021).
49. D. M. Pozar, *Microwave Engineering* (John wiley & sons, 2011), 4th ed.
50. C. A. Balanis, *Antenna theory: analysis and design* (John wiley & sons, 2016), 2nd ed.